UNDERSTANDING THE TOUGHNESS MECHANISM PROMPTED BY SUBMICRON RIGID PARTICLES IN POLYLACTIDE/BARIUM SULFATE COMPOSITES

N. Sadaba[1], R. Martini[2], F. Barthelat[2], I. Martínez de Arenaza[1], A. Larrañaga[1], J. R. Sarasua[1], E. Zuza[1]*

[1]University of the Basque Country (UPV/EHU), Department of Mining-Metallurgy Engineering and Materials Science & POLYMAT, Faculty of Engineering, Alameda de Urquijo s/n 48013 Bilbao, Spain

[2] McGill University, Department of Mechanical Engineering, Laboratory for Advanced Materials and Bioinspiration, Montreal, Canada

* e-mail: ester.zuza@ehu.eus

Abstract

Polylactides are extensively employed as bone-fixation devices, due to their degradability and high tensile modulus. As demonstrated in a previous study, the incorporation of barium sulfate submicron particles impressively enhanced toughness with almost no adverse effect on yield strength. It is therefore a promising strategy in the design of radiopaque materials intended for use in safety-critical systems. In the present study, the mechanism that causes high-level plastic deformation in this system is identified through tensile and fracture tests, together with a thorough analysis of the microstructure via transmission and SEM (Scanning Electron Microscopy). The presence of submicron particles was observed to reduce crystallinity and to increase energy dissipation during the plastic deformation of the polymer matrix, inducing crack widening and fibrillated crazing that propagated around the crack opening. The result is a five-fold increase in the energy that is required to fracture the composite with respect to its neat polymer counterpart.

1. Introduction

Polylactides (PLAs) are degradable and have shown excellent biocompatibility in many biomedical applications such as scaffolds for tissue regeneration [1-3], drug delivery vehicles [4,5], sutures [6,7], and implants [8]. Regarding the mechanical properties of the polymers, PLAs display a high tensile modulus (3 GPa [9]) and yield strength (50-70 MPa [10]), but little elongation at breakage points (5-7%), which implies a brittle behavior of the polymer with no region of plastic deformation. Therefore, strategies that can increase the toughness of fragile polymers are of tremendous interest when these materials are intended for use in safety-critical systems, such as bone fixation devices, where increased polymer toughness remains a central challenge [11]. In particular, the fracture properties of PLAs play a key role in the successful implantation of many implanted devices and, in consequence, in their long-term survival (e.g. fixation devices) [12].

Many strategies have been proposed in the literature (e.g., blending with an impact modifying rubber phase, plasticization, incorporation of inorganic particles, etc.), in order to overcome the brittleness associated with PLAs, [13,14]. Blending with rubber-like polymers, which leads to a toughened second phase, is one of the most commonly employed approaches to improve the ductility of brittle polymers [15]. It has been widely reported that this increment is induced by the crazing mechanism, as demonstrated in rubber-modified high-impact polymers, such as high impact polystyrene (HIPS) [16], acrylonitrile-butadiene-styrene (ABS) [17], and high impact polymethyl methacrylate (PMMA) [18]. However, this strategy adversely affects yield strength and, consequently, the mechanical properties of the material [19]. In contrast, some researchers have demonstrated that improved ductility in PLAs, due to

plasticization, implies a lowering of T_g to at least 35 ºC. Such a large decrease affects compressive strength and the modulus of tensility, especially when the polymers are designed for use inside the human body [20]. A combined approach has also been reported, in which rubber and rigid particles are simultaneously incorporated that improve both the toughness and the stiffness of the polymer matrix, respectively [21]. However, this solution will not solve the problem of ageing, which induces migration of plasticizer, phase separation, and changes in physical properties over time [22]. Additionally, blending with immiscible polymers represents a more efficient strategy to increase the ductility and the toughness of PLAs than their blending with miscible counterparts, due to the creation of a two-phase morphology [23,24]. In general, the incorporation of a rubber phase increases ductility and toughness, but decreases Young's modulus and yield strength.

Ritchie [25] demonstrated that the deformation capacity of a material before rupture is a critical aspect of conferring toughness, as the deformation process enables the local dissipation of high stresses, which otherwise would result in material fracture. In the same study, he proposed two mechanisms for local dissipation: one intrinsic and another extrinsic. The intrinsic mechanism works ahead of the crack tip and it has a particular size (<1 μm), the essential function of which is to induce plasticity. This mechanism affects the initiation and the growth phase of the crack. However, the extrinsic mechanism (that is behind the crack) lowers local stress at the crack tip. Its effects limit themselves to crack-growth toughness and it depends on the presence of the crack.

Biomimetic approaches serve as a source of inspiration, from which similar concepts can be translated into artificial systems, thereby developing materials with improved performances. For example, bone toughness is associated with a fibrillar sliding

4

mechanism, inhibited by cross-linking of collagen, which constrains the movement of the fibrils reducing the toughness of the bone, for example when bone is irradiated or suffers certain diseases [26,27]. Toughness in nacre is explained by allowing some movement between mineral platelets and this property is lost when movement is limited to 1 μm [28]. Based on the fibrillar sliding mechanism and the movement of platelets, both Gupta [29] and Barthelat [28] concluded that, although the conflicts between the generally exclusive properties of strength and toughness are substantial (because toughness is obtained with high strength and high ductility, qualities which are difficult to find in the same material), there are ways to promote toughness. It can be achieved through the presence of multiple plasticity and toughening mechanisms acting on different length scales.

$BaSO_4$ has for many years been used in biomaterials as a radiopacifier in bone cements for dental and orthopedic applications [30,31], In general, $BaSO_4$ particles produce mechanical weakness in bone cements, mainly if higher proportions of particles are used.

In our previous work, $BaSO_4$ submicron particles were incorporated in PLA to confer radiopacity to the resulting composite [32]. Ductility of the polymer matrix was impressively enhanced (from 3.9 % to 134%) by the incorporation of 10% $BaSO_4$ submicron particles with no apparent detrimental effect on yield stress (70.2 MPa to 67.6 MPa). However, this mechanism remains unexplained in barium sulfate containing composites just as it does in particulated composites in which a neat fragile matrix and is turned into a ductile one.

Hence, this strategy is of particular interest for the manufacture of materials that are intended for use in safety-critical applications, such as bone fixation devices, or new trending 3D-printable pieces.

The main aim of the present work is to elucidate the microscale and/or nanoscale mechanisms that promote high levels of plastic deformation in PLA/ $BaSO_4$ composites. Its novelty is related to the increased toughness of polylactide matrices through the incorporation of a rigid phase consisting of inorganic particles.

2. Experimental

Commercial poly(D-lactide) PDLA (100,000 g mol^{-1}) was kindly provided by PURAC BIOCHEM in the form of pellets and barium sulfate ($BaSO_4$) inorganic salt was supplied by Sigma-Aldrich in powder form. The $BaSO_4$ particle size distribution was estimated by means of Optical Vertical microscopy for material analysis with universal LED illumination (Leica DM LM) images, together with the image processing software ImageJ (free software). Thermal analyses were performed with a DSC from TA Instruments, model DSC 2920 with a scan rate of 20 C/min, up to 200 ºC.

PDLA/$BaSO_4$ composites containing 0.5, 1, 2, 5 and 10.0 wt.% of $BaSO_4$ were fabricated using a melt blending method in a Vertical DSM Xplore Model 5 mini-mixer. Two types of specimen geometry were fabricated: dumbbell-shaped specimens for uniaxial tensile tests using a Xplore micro injection molder Machine (IM 12) 12cc (Xplore Instruments BV) and compact tension specimens for fracture toughness tests using compression molding. The mold used for injection had a geometry for tensile test specimens. Hence the use of compression molding to fabricate the samples for fracture

toughness analysis. Tensility testing revealed that the samples manufactured by micro injection or compression molding had similar mechanical properties. The dimensions of the specimens are shown in Figure 1.

Tensile tests were performed on 1 mm thick specimens using an Instron 5565 testing machine with a maximum load of 500 N and a crosshead displacement rate of 5 mm min^{-1} (leading in a %strain/time of 12.5%/min). The mechanical properties of the specimens were measured at 21 ± 2 ºC and 50 ± 5 % relative humidity (RH) following ISO 527-2/5A/5/1995 one day after processing, to ensure that all the samples would be left for similar intervals of time between processing and testing. The mechanical properties reported for each material correspond to average values of five experiments.

Fracture tests were performed on a miniature loading machine (E. Fullam, NY) at a rate of 1.2 mm min^{-1}, where the tensile force was transmitted by two pins.
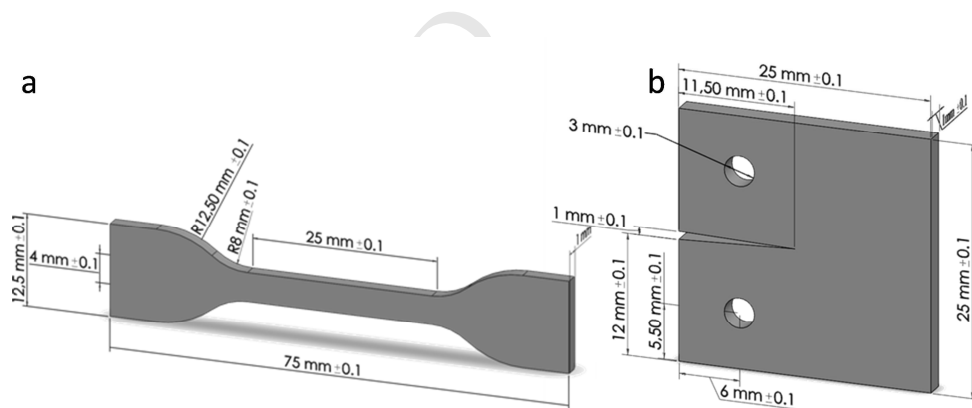

Figure 1. Specimen geometry for (a) uniaxial tensile tests (dumbbell-shaped sample); and, (b) fracture toughness tests (compact tension sample); both samples with a thickness of 1mm .

Scanning and transmission electron microscopy (SEM, JEOL JSM-6400 with a W filament and a resolution of 3.5 nm and TEM, TECNAI G2 20 TWIN under an accelerated voltage of 200 kV) were used to study the morphology of the composites and the dispersion of the $BaSO_4$ particles in the polymer matrix. SEM images collected

by primary (backscattered) electrons highlighted high mass elements and, consequently, the distribution of the $BaSO_4$ particles within the polymer matrix was easily determined. In contrast, SEM images recorded with secondary electrons revealed the morphology of the fracture mechanism surface under study. The stress lines were observed in the cryogenically sectioned samples that had been immersed in liquid nitrogen for 2-3 minutes, quickly marked with a razor blade in the stress direction, and then hammered until fracture.

3. Results and discussion

3.1. $BaSO_4$ particle size distribution and dispersion in a PDLA matrix

The $BaSO_4$ particles in this study displayed a distribution with a mean particle size of 0.75 µm (Figure 2).
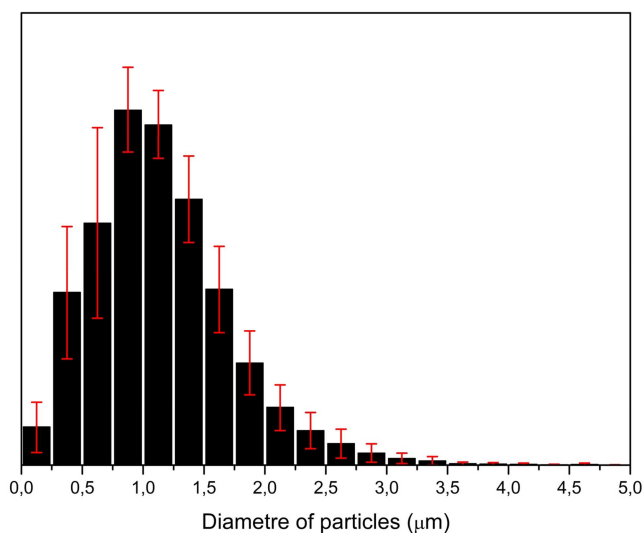

Figure 2. Size distribution of $BaSO_4$ particles as received.

As observed in Figure 3, the BaSO$_4$ particles appeared to be well dispersed within the PDLA matrix after melt blending, with no aggregation larger than a particle size of 2 µm.
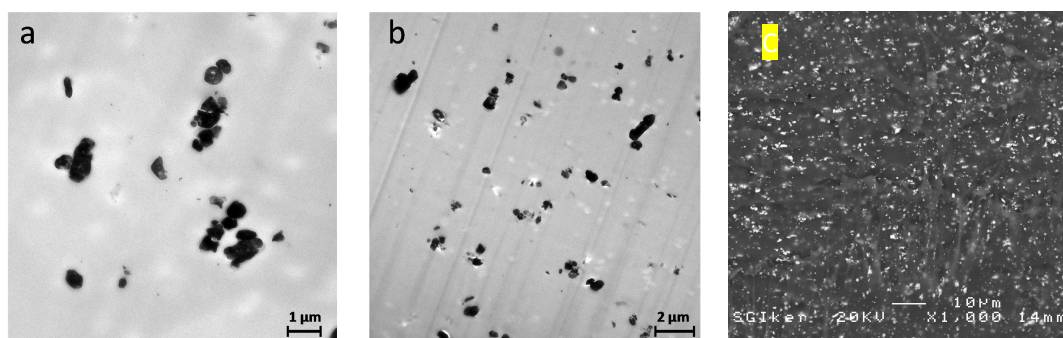

Figure 3. TEM images showing (a,b) agglomeration; and SEM image showing (c) dispersion of PDLA loaded with 10 wt.% BaSO$_4$ particles.

3.2. Influence of rigid particles on polylactide crystallization

Calorimetric analysis confirmed that the presence of barium sulfate particles affected polylactide crystallinity, as can be observed in Table 1. The incorporation of particles reduced the crystallinity of the matrix (from 14 to 8.5%). One consequence of the reduction of the crystalline fraction was that the amorphous region increased, affording further mobility the polymer segments. Other authors reported similar behavior with the incorporation of BaSO$_4$ in polypropylene [33], stating that the reduction in crystallization capability is directly related with matrix/particle interactions.

BaSO$_4$ (%)	Crystallinity of polylactide fraction (%)
0	14.0
10	8.5

Table 1. Influence of barium sulfate particles on polylactides crystallinity.

3.3. Tensile tests

Figure 4 shows the typical tensile stress-strain curves and the bar plots of the mechanical parameters for samples loaded with 0 (neat matrix) and 10 wt.% of $BaSO_4$ particles. As observed in our previous study [31], the incorporation of $BaSO_4$ submicron particles impressively increased the elongation at break and the corresponding toughness of the PLA matrix. This greater toughness was accompanied by a slight decrease in the observed yield strength. Hence, the rigid particles clearly played an important role in both the deformation and the rupture mechanisms of the PDLA. Further analysis was therefore conducted to investigate the way that these particles influenced the behavior of the composites: fracture toughness and surface morphology tests as well as tests on interior surface areas of specimen pieces broken in the tensile tests.
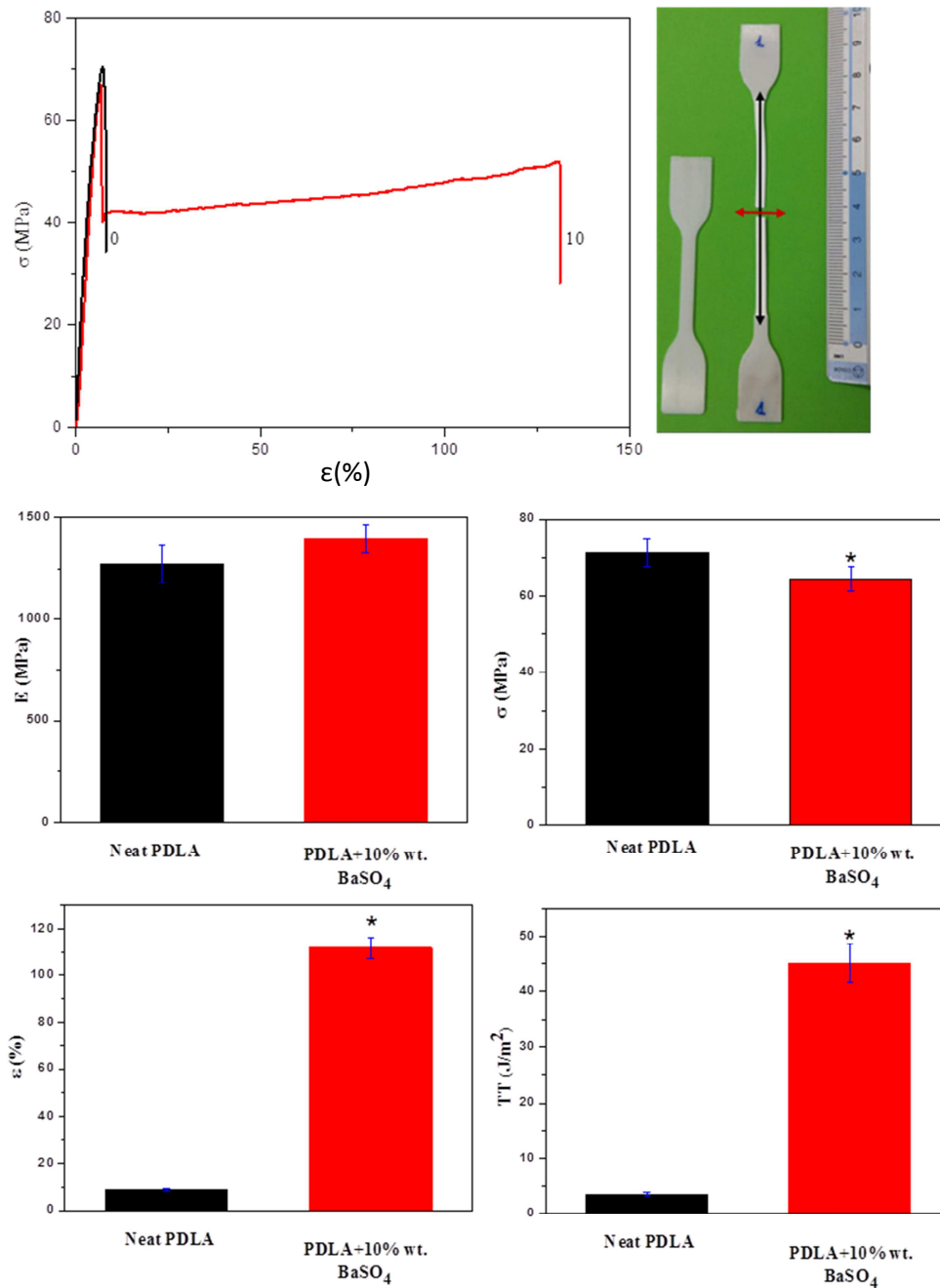
Figure 4. Results of tensile tests and mean values ± SD for neat PDLA (black) and PDLA composite

filled with 10 wt. % of BaSO$_4$ (red): a) stress-strain curves; b) specimen of PDLA composite after

rupture; c) elastic modulus (E); d) yield strength (σ); e) ultimate strain (ε) and f) tensile toughness (TT).

Statistically significant differentiations have been marked with an asterisk.

3.4. Fracture toughness test

All the samples tested in this study showed stable crack propagation patterns. Figure 5a shows the typical force-deflection curves for fracture tests on neat PDLA and PDLA+10 wt.% $BaSO_4$. The bell shape of the curve also indicates stable crack propagation in both types of materials. Initially the response was linear, up to a maximum force where stable crack propagation started. Failure was then progressive until complete fracture of the sample. A slightly higher force was required to propagate the crack in PDLA+10 wt.% $BaSO_4$, but the fractured sample withstood further deformation, and the energy required for fracture was much greater than the neat PDLA. Figure 5b shows a set of typical images acquired during the tests. For both materials, a region of plastically deformed material could be seen ahead of the initial notch, in the form of stress whitening (black arrows in Figure 5b). The plastic zone on neat PDLA was small and relatively homogenous. For PDLA+10 wt.% $BaSO_4$, the plastic region was significantly larger in size, and displayed branches that are typical of materials that soften upon deformation. Once the crack propagated through this region of stress-whitening, a permanently deformed region remained near the crack faces in the wake of the crack (see Figure 5b lower row E). The wake was more difficult to observe in situ on the PDLA+10 wt.% $BaSO_4$, sample because of warping and out-of-plane deformations.
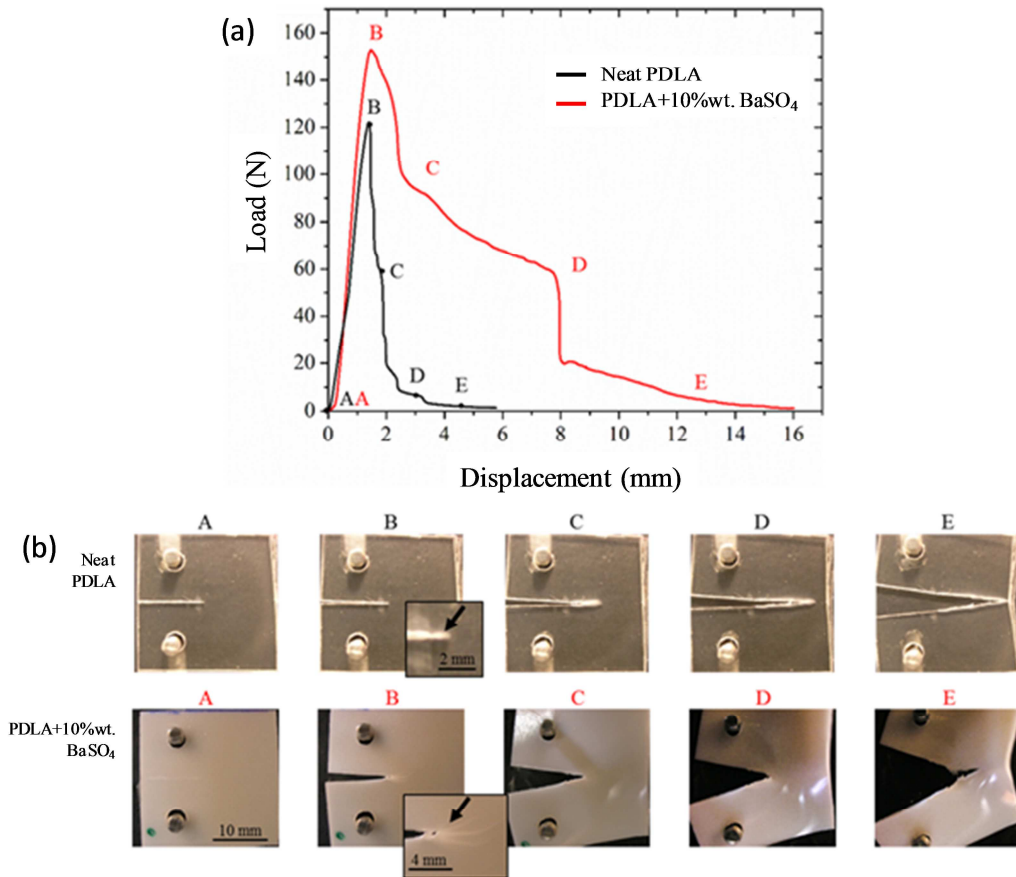
Figure 5. (a) Typical force-displacement curves obtained from fracture tests on neat PDLA and PDLA+10 wt.% $BaSO_4$. (b) Optical images of these two materials acquired during the fracture tests showing the points (A,B,C,D,E) indicated on the force-displacement curve. Inset in B shows the presence or otherwise of branches.

Figure 6 shows a comparison of the fracture properties. The force to initiate crack propagation (F_{max}) is roughly 25% greater in PDLA+10 wt.% $BaSO_4$ than in neat PDLA. As the nonlinear regions of the sample are large no estimate of fracture toughness is given. Instead, a work of fracture (w.o.f.) was calculated by dividing the area under the force-displacement curve by the cross section of the ligament of material ahead of the notch (cracked material), therefore, the w.o.f. measures the energy that is needed to propagate the crack and then to break the material.
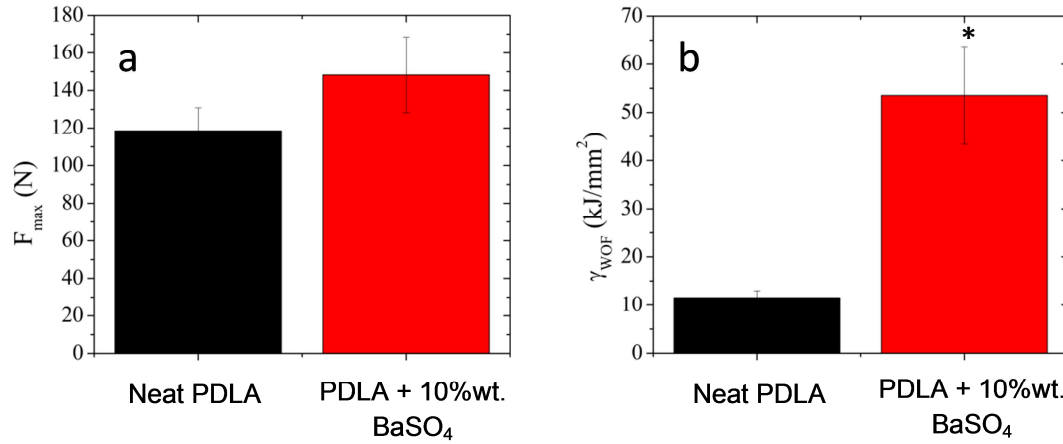
Figure 6. Comparison of fracture properties between neat PDLA and PDLA+10 wt% BaSO$_4$ (a) comparison of crack propagation initiation forces; (b) comparison of work of fracture.

Figure 6b shows that the w.o.f of PDLA+10 wt.% BaSO$_4$ is five times higher than the w.o.f. of neat PDLA, which is a remarkable improvement by any standard. It is hypothesized that this improvement in toughness is due to the energy absorbed by the material ahead of the crack tip and behind it in the wake region. In addition to the plastic deformation of PDLA, PDLA+10 wt.% BaSO$_4$ composite can dilate due to particle debonding and cavity growth, a micro-mechanism which is similar to rubber-toughened epoxy [15]. The amount of toughening generated by the process zone may be estimated from the tensility of the material and from the width of the wake of inelastically deformed material. The increased toughness ΔJ (in terms of energy) in the process zone can be expressed as follows [15]:

$$\Delta J = 2\int_0^w U(y)dy$$

Where $U(y)$ is the energy density dissipated by plastic deformation in the wake of the crack, y is the distance from the crack face, and w is half width of the process zone. On the assumption that $U(y)$ decreases linearly from a maximum value (U_{max}, at $y = 0$

where the tensile strain is maximum ($\varepsilon = \varepsilon_{max}$)) to zero (at $y = w$, edge of the process zone), the model simplifies to:

$$\Delta J = w U_{max}$$

Here, U_{max} is the area under the stress-strain curve shown in figure 4a, which can be estimated for the PDLA+10 wt.% BaSO$_4$ material as $U_{max} \approx \sigma_y \varepsilon_{max}$ when σ_y is the yield strength and ε_{max} is the maximum tensile strain. Using $\sigma_y \approx 40\,\mathrm{MPa}$ and $\varepsilon_{max} \approx 1.25\%$ from the tensile data on the PDLA+10 wt.% BaSO$_4$ material yielded a value of $U_{max} \approx 50\mathrm{MJ/m}^3$. In turn, the half-width of the process zone measured experimentally for PDLA+10 wt.% BaSO$_4$ was $w \approx 2\,\mathrm{mm}$, so that the contribution of the process zone to toughness for this material was $\Delta J \approx 100$ kJ/m^2. This prediction is higher than the experimentally measured toughness of the material ($J \approx 60$ kJ/m^2), which may be explained by the assumption made on the energy distribution in the wake. Nevertheless, the model demonstrates that process zone mechanisms can be a major source of toughness for the material. In comparison, the half-width of the process is only 0.5 mm for plain PDLA, and the strain at failure is much lower ($\varepsilon_{max} \approx 0.1$). Consequently, the model predicts a toughness increment of only $\Delta J \approx 0.5$ kJ/m^2 for this material. Experimental observation and the model presented here strongly suggest that the inelastic deformations developing ahead and behind an advancing crack in PDLA+10 wt.% BaSO$_4$ are the main sources of toughening, through process-zone mechanisms similar to those in rubber toughened epoxies [15].

3.5. Fracture surface and internal morphology analysis

The results obtained in the mechanical fracture tests confirmed that particles are involved in the energy dissipation contribution and physically contribute to the toughening of the PDLA. Therefore, the analysis of their microscale images will yield further details of the toughening mechanism.

The images of fractured surfaces following tensile tests are shown in Figure 7. PDLA without particles shows an unwrinkled surface and the width of the sample is similar to that of the specimen before the tensile-test. In contrast, the composite with 10 wt.% of $BaSO_4$ tears (Figure 7 C), leading to a highly deformed and rough surface with a clearly smaller thickness than that of the specimen before the tensile-test.
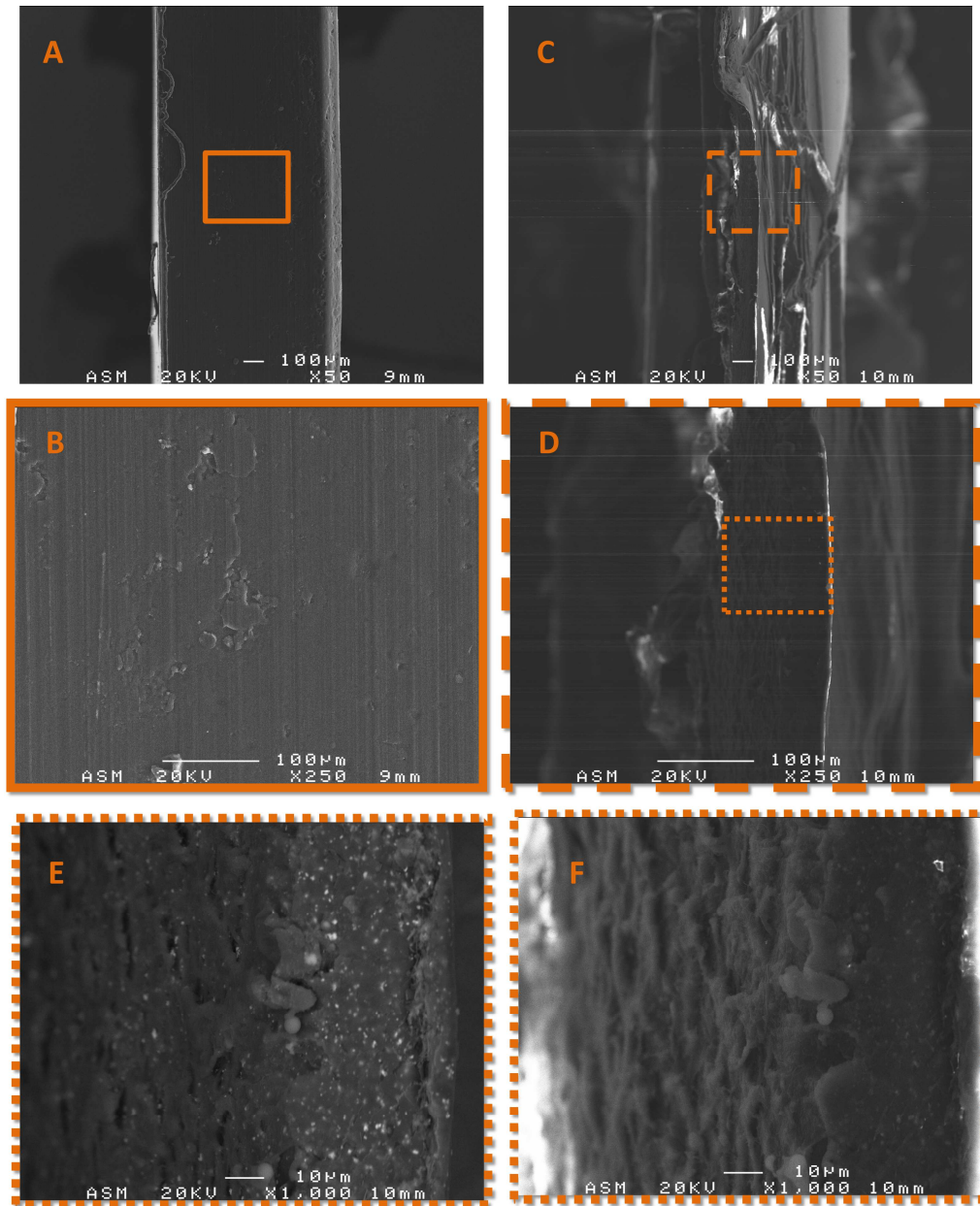
Figure 7. Surface fracture of PDLA samples containing 0 (A,B) and 10 wt.% (C,D,E,F) of $BaSO_4$ particles. A and C are images with a magnification of x50, and B and D are the corresponding zoomed zones highlighted with a rectangle. E and F are magnified images of D collected with secondary and primary electrons, respectively.

Composites with lower percentages of $BaSO_4$ (0.5 and 2 wt.%) are analyzed for a better understanding of the deformation mechanism. In both cases similar mechanical behavior to that of samples filled with 10 wt.% of $BaSO_4$ particles was observed, but the presence of smaller amounts of rigid particles help us to understand the fracture

17

mechanism better (i.e., how the voids are generated and how these voids turn into crazing) because the particles form no overlapping mechanisms. To distinguish between void generation and the development of crazes, SEM images were taken at different positions on the fractured surface: one position is (approx. 10 mm) away from the rupture and is expected to depict an earlier stage of the mechanism (initiation of debonding of the particles and cavitation of voids, pointed out as 1 in Figure 8); the other position is near (within 1 mm from) the rupture zone in which a more advanced stage of the deformation is foreseen (deformed voids and the initiation of craze formation, see image 2 in Figure 8).
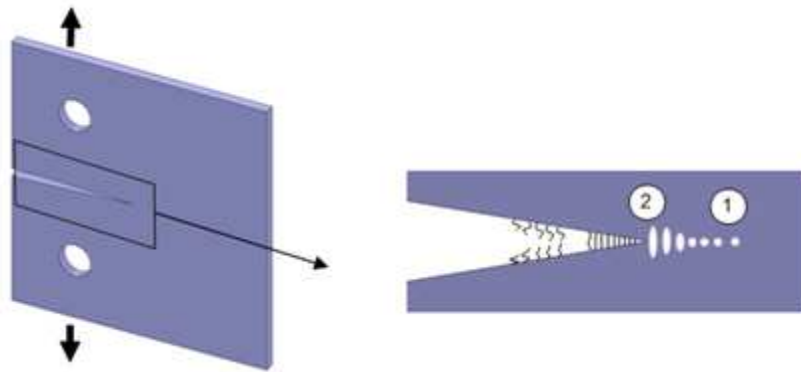

Figure 8. Schematic representation of the steps involved in the crazing process. 1) earlier stage: debonding and cavitation of the voids; 2) advanced stage: deformed voids initiate craze formation.

Figure 9 shows images of a zone of the specimen that is far (approx. 10 mm) from the rupture (Figure 9A), in which the width shows similar thickness to that of the initial sample. Figures 9C and 9E show particles as void initiators; an effect that is more obvious in Figure 9D, where highlighted fillers are positioned within dark holes.

In contrast, Figure 10 shows SEM micrographs that were taken in a zone that was closer to the rupture area (pointed out as 2 in Figure 8). In this case, the particles were not found within voids, that evolved toward larger holes, thus forming an interconnected network and collapsing. This behavior results in craze formation. Figure 10B shows

voids separated by fibrils along the craze interfaces (highlighted with white arrows in Figure 10B).
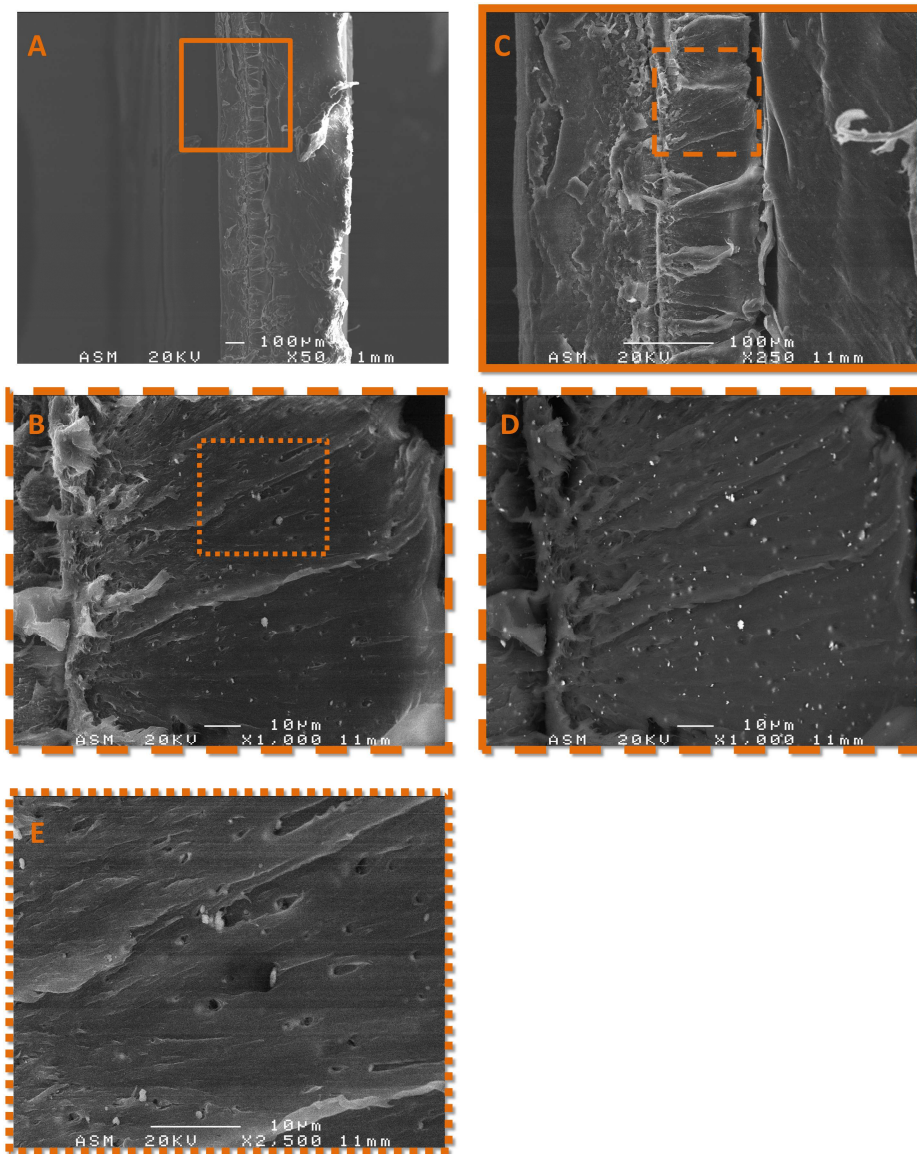

Figure 9. Fracture surface images of PDLA tensile specimen filled with 2 wt.% of BaSO$_4$. 10A and 10B indicate the area under study. 10C, 10D and 10E show particles inside voids.
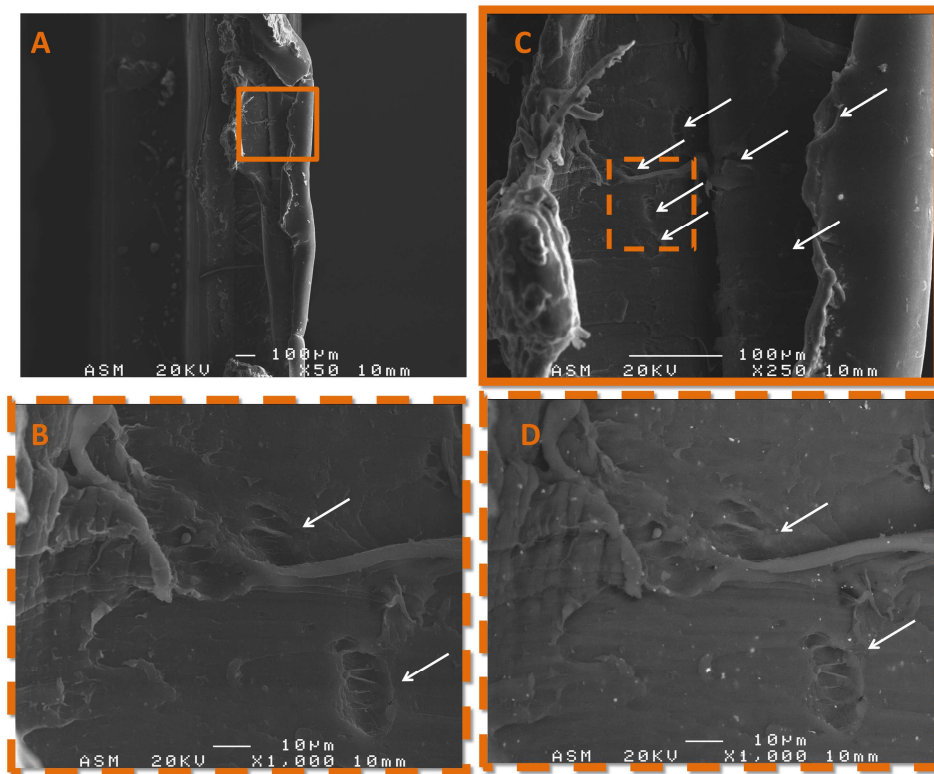
Figure 10. Fracture surface images of PDLA specimen with 0.5 wt.% of $BaSO_4$ under tensile stress: A and B with magnifications of x50 and x250, respectively; C and D are magnified images of B collected with secondary and primary electrons respectively.

Moreover, for a better understanding of the deformation mechanism initiated by particles, cryogenically ruptured samples in the stress direction were analyzed. Figure 11 shows SEM micrographs of those composites with 10 wt.% $BaSO_4$ particles: SEM images reveal the surface morphology when it is collecting secondary electrons (in figures 11 A and 11 B), rather than primary electrons which reveal images of deeper sub-surface zones that highlight higher mass atomic elements. In Figure 11B large voids are observed, which induce highly deformed fibrils in the stress direction resulting in a fibrillated structure. The diameters of the fibrils vary from 1 to 6 µm and the dimensions are characteristic of plastic deformation [34]. Figures 11C and 11D also highlight the good dispersion of $BaSO_4$ particles in the PDLA matrix as previously observed via TEM analysis (Figure 3).
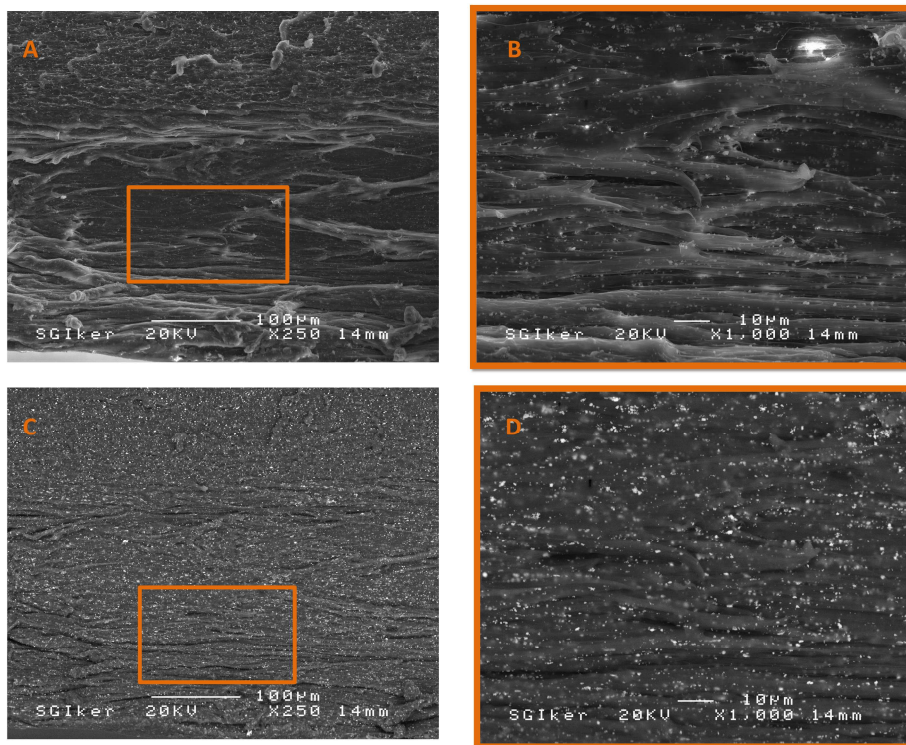
Figure 11. Cryogenic rupture of PDLA with 10 wt.% BaSO$_4$. A and B (zoomed images) correspond to images collected by secondary electrons. In contrast, C and D (zoomed images) are collected with primary electrons. Stress direction is horizontal.

5. Conclusions

BaSO$_4$ has been blended with polymethylmethacrylate (PMMA), extensively used for years as radiopacifier in bone cements for arthroplasty and dentistry applications [30,31]. PMMA is a brittle polymer and the incorporation of barium sulfate particles in no way changes its mechanical properties, as it remains weak. Hence, Lissarrague et al. proposed the synthesis of branched polymers, which increase strength and modulus while strain at break and wear resistance were negatively affected. The authors explain this behavior by the existence of weak linking zones between the nanoparticles and the

polymer matrix [35]. In summary, the interface between $BaSO_4$ and PMMA composite is poor and the mechanical behavior of the matrix composite remains fragile.

Other recent studies have demonstrated good physical interactions between $BaSO_4$ and poly(ethylene-vinylacetate) copolymers that permit a better dispersion of the particles and a higher incorporation of radiopaque particles in the matrix [36]. However, mechanical properties of neat copolymer are ductile and the incorporation of $BaSO_4$ particles in no way change the mechanical properties.

In the particular case considered in this study, the addition of submicron $BaSO_4$ particles led to well dispersed voids in PDLA, regardless of the amounts of particles. Rigid particles are known to act as discontinuities in polymer matrices and will therefore create voids or defects in the polymer structure when the material is under tensile stress [37]. Good dispersion in a composite material depends on the establishment of physical interactions between the sulfate particle groups and the ester group of the matrix, promoting a good interface, similar to the ester groups in acetate units observed by Lissarrague et al. These interactions between particles and matrix also reduce matrix crystallinity. They therefore increase the movement of the polymer chains, favoring the high deformation values that have been observed in mechanical testing.

The mechanical behavior of the composites is also enhanced when a composite is subjected to a mechanical stress: elongation of particle-created voids occurs in the stress direction and elliptical holes and a fibrillated matrix is developed. Therefore, the mechanism initiated by particle debonding (Figure 9) continues with craze formation and finally results in high deformation values. However, this mechanism has neither been previously explained for barium sulfate containing composites, nor for other composites in which the neat matrix is fragile and its particulated composite becomes

22

ductile. This behavior was observed in this study as rubber or void toughening strategies that have previously been reported as a mechanism that influences the local stress state [38].

In any event, the improvement of toughness is due to the energy absorbed by the material ahead of the crack tip and behind it in the wake region. Accordingly, particular attention must be paid to the submicron size and the round shape of the fillers. These well dispersed submicron voids favor the activation of intrinsic and extrinsic mechanisms. Thus, this study has successfully reported high deformation of a brittle matrix that is achieved without any need to incorporate a rubber phase.

Acknowledgements

References

[1] S.S. Silva, J.F. Mano, R.L. Reis, Potential applications of natural origin polymer-based systems in soft tissue regeneration, Crit. Rev. Biotechnol. 2010, 30,200-221.
[2] J.R. Sarasua, N. Lopez-Rodriguez, E. Zuza, S. Petisco, B. Castro, M. del Olmo, T. Palomares, A. Alonso-Varona, Crystallinity assessment and in vitro cytotoxicity of polylactide scaffolds for biomedical applications. J Mat Sci-Mat M 2011, 22, 2513-2523.
[3] A. Larrañaga, A. Alonso-Varona, T. Palomares, E. Rubio, P. Aldazabal, F.J. Martin, J.R. Sarasua, Effect of bioactive glass particles on osteogenic differentiation of adipose-derived mesenchymal stem cells seeded on lactide and caprolactone based scaffolds, J. Biomed. Mater. Res. Part A 2015.
[4] H. Tian, Z. Tang, X. Zhuang, X. Chen, X. Jing, Biodegradable synthetic polymers: preparation, functionalization and biomedical application. Prog. Polym. Sci. 2012, 37, 237-280.

[5] B. Tesfamariam, Bioresorbable vascular scaffolds: Biodegradation, drug delivery and vascular remodeling. Pharmacological Research 2016, 107, 163–171.

[6] B. Gupta, N. Revagade, J. Hilborn, Poly(lactic acid) fiber: An overview. Prog. Polym. Sci. 2007, 32, 455-482.

[7] T. Maharana, B. Mohanty, Y. S. Negi, Melt–solid polycondensation of lactic acid and its biodegradability. Prog. Polym. Sci. 2009,34,99–124.

[8] J.C. Middleton, A.J. Tipton, Synthetic biodegradable polymers as orthopedic devices. Biomaterials 2000, 21, 2335-2346.

[9] J.S. Bergstroem, D. Hayman, An Overview of Mechanical Properties and Material Modeling of Polylactide (PLA) for Medical Applications. Annals Of Biomedical Engineering 2016, 44, 330-340.

[10] A. Sodergard, M. Stolt, Poly (Lactic Acid) Production for Tissue Engineering Applications, Prog. Polym. Sci. 2002, 27, 1123-1163.

[11] S. Farah, D.G. Anderson, R. Langer, Physical and mechanical properties of PLA, and their functions in widespread applications — A comprehensive review. Advanced Drug Delivery Reviews 2016, 107, 367-392.

[12] J.M. Ugartemendia, A. Larrañaga, H. Amestoy, A. Etxeberria, J.R. Sarasua, Tougher biodegradable polylactide system for bone fracture fixations: Miscibility study, phase morphology and mechanical properties. European Polymer Journal 2018, 98, 411-419.

[13] K.S. Anderson, K.M. Schreck, M.A. Hillmyer, Toughening polylactide, Polymer Reviews 2008,48(1),85-108.

[14] V. Nagarajan, A.K. Mohanty, M. Misra, Perspective on Polylactic Acid (PLA) based Sustainable Materials for Durable Applications: Focus on Toughness and Heat Resistance, ACS Sustainable Chemistry & Engineering 2016,4(6),2899-2916.

[15] A.G. Evans, Z.B. Ahmad; D.G. Gilbert; P.W.R. Beaumont, Mechanisms of toughening in rubber toughened polymers, Acta Metall. 1986, 34, 79-87.

[16] L.D. Zhu, H.Y. Yang, G. Di Cai, Z. Chao, G. F. Wu, M.Y. Zhang, G. H. Gao, H. X. Zhang, Toughened Isotactic Polypropylene: Phase Behavior and Mechanical Properties of Blends with Strategically Designed Random Copolymer Modifiers. Journal of Applied Polymer Science 2013, 129, 224-229.

[17] M. Helbig, E. van der Giessen, A. H. Clausen, T. Seelig, Continuum-micromechanical modeling of distributed crazing in rubber-toughened polymers. European Journal of Mechanics A-Solids 2016, 57,108-120.

[18] L. Lalande, C. J. G. Plummer, J. A. E. Manson, P. Gerard, The influence of matrix modification on fracture mechanisms in rubber toughened polymethylmethacrylate. Polymer 2006, 47, 2389-2401.

[19] G. H. Michler, F.J. Baltá-Calleja, Rubber Toughened Polymers, In Nano- and Micromechanics of Polymers, Hanser, 2012, 315-368.

[20] M. Baiardo, G. Frisoni, M. Scandola, Thermal and mechanical properties of plasticized poly(L-lactic acid). Journal of Applied Polymer Science 2003, 90, 1731–1738.

[21] M. Pluta, M.A. Paul, M. Alexandre, P. Dubois, Plasticized polylactide/clay nanocomposites. II. The effect of aging on structure and properties in relation to the filler content and the nature of its organo-modification. Journal of Polymer Science: Part B: Polymer Physics 2006, 44, 312–325.

[22] N. Lopez-Rodriguez, A. Lopez-Arraiza, E. Meaurio, J.R. Sarasua, Crystallization, morphology, and mechanical behavior of polylactide/poly(ε-caprolactone) blends. Polymer Engineering And Science 2006,46 (9)1299-1308.

[23] H. Liu, J. Zhang, Research Progress in Toughening Modification of Poly(lactic acid). J Polym Sci Part B Polym Phys 2011, 49, 1051–1083.

[24] E. Meaurio, N. Hernandez-Montero, E. Zuza, J.R. Sarasua, In: Characterization of Polymer Blends: Miscibility, Morphology and Interfaces. Thomas, S; Grohens, Y; Jyotishkumar, P Ed.; 2015, Vol. 1, p 7-92.

[25] R.O Ritchie, The conflicts between strength and toughness. Nature Materials. 2011, 10, 817-822.

[26] R.K. Nalla, J. H. Kinney, R. O. Ritchie, Mechanistic fracture criteria for the failure of human cortical bone. Nature Mater. 2003, 2, 164–168.

[27] K.J. Koester, J.W. Ager, R.O. Ritchie, The true toughness of human cortical bone measured with realistically short cracks. Nature Mater. 2008,7, 672–677.

[28] F. Barthelat, H. D. Espinosa, An Experimental Investigation of Deformation and Fracture of Nacre–Mother of Pearl. Exp. Mech. 2007, 47, 311–324.

[29] H.S. Gupta, W. Wagermaier, G.A. Zickler, D. R.-B. Aroush, S.S. Funari, P. Roschger, H. D. Wagner, P. Fratzl, Nanoscale Deformation Mechanisms in Bone, NanoLetters 2005, 5, 2108-2111.

[30] E. J. Tobin, Recent coating developments for combination devices in orthopedic and dental applications: A literature review, In Advanced Drug Delivery Reviews, Volume 112, 2017, Pages 88-100.

[31] M. Arora, E. K. Chan, S. Gupta, A. D. Diwan, Polymethylmethacrylate bone cements and additives: A review of the literature. World Journal of Orthopedics, 2013, 4(2), 67–74.

[32] I. Martínez de Arenaza, N. Sadaba, A. Larrañaga, E. Zuza, J.R. Sarasua, High toughness biodegradable radiopaque composites based on polylactide and barium sulfate. European Polymer Journal 2015, 73, 88–93.

[33] A. Pawlak, A. Galeski, A. Rozanski, Controlling Cavitation of Semicrystalline Polymers during Tensile Drawing. *Prog. Polym. Sci.* 2014, 39, 921-958.

[34] M. H. Lissarrague, M.L. Fascio, S. Goyanes, N.B. D'Accorso, Improving bone cement toughness and contrast agent confinement by using acrylic branched polymers. *Materials Science and Engineering C* 2016, 59, 901–908.

[35] S.K. Suman, R.K. Mondal, J. Kumar, K.A. Dubey, R.M. Kadam, J.S. Melo, Y.K. Bhardwaj, L. Varshney, Development of highly radiopaque flexible polymer composites for X-ray imaging applications and copolymer architecture-morphology-property correlations. *European Polymer Journal* 2017, 95, 41-55.

[36] G.H. Michler, H.H. Kausch, B. von Schmeling, The physics and micro-mechanics of nano-voids and nano-particles in polymer combinations. *Polymer* 2013, 54, 3131-3144.

[37] W.G. Perkins, Polymer toughness and impact resistance. *Polymer Engineering and Science* 1999, 39, 2445.

[38] R.J.M. Borggreve, , R.J. Gaymans, J. Schuijer, Impact behaviour of nylon-rubber blends: 5. Influence of the mechanical properties of the elastomer. *Polymer* 1989, 30, 71–77.

- Submicron rigid particles induce toughness in polylactides

- Debonding of particles and cavitation of voids iniciate crazing mechanism

- Inelastic deformation ahead and behind the crack leads into toughness of matrix

- promising radiopaque and tough biomaterials for medical devices

- presence of rigid particles changes from fragile behavior to a ductile matrix